Direct and large-eddy simulation of transient buoyant plumes : a comparison with an experiment

Direct and Large-Eddy Simulation of Transient Buoyant Plumes: A Comparison with an Experiment

R.J.M. BASTIAANS, C.C.M. RINDT and A.A. VAN STEENHOVEN
J.M. Burgers Centre for Fluid Mechanics, Eindhoven University of Technology
Dept. Mechanical Engineering, P.O.box 513, 5600 MB Eindhoven, The Netherlands.

and

F.T.M. NIEUWSTADT
J.M. Burgers Centre for Fluid Mechanics, Delft University of Technology
Lab. Aero- and Hydrodynamics, Rotterdamseweg 145, 2628 AL Delft, The Netherlands.

Abstract. In the present study transitional thermal plumes are examined by means of numerical simulations and experiments. The objective of the research is the determination whether a Large-Eddy Simulation can be applied in these cases and what subgrid scale model should be used. The Prandtl number is 5.82. Results are obtained in terms of the topology of a two dimensional slice of the temperature field and the local temperature and velocity as function of time. Experimentally the topology of the temperature field was obtained using liquid crystals suspended in water; the local temperature was measured with a thermocouple. Numerically, two- and three-dimensional calculations were performed, using the subgrid turbulent kinetic energy model, as used by Nieuwstadt [10], and the Smagorinsky [12] model. In the two dimensional case also direct numerical simulations were performed.

1 Introduction

Transitional thermal plumes occur quite frequently in nature and technical devices. Examples are the flow induced by a cigarette (naturally visualized), plumes arising (or descending) from spiral heat exchangers and plumes generated by electronic components. The interest for studying these flows is mostly the need to maximize or minimize total heat transfer or to reduce entropy production due to mixing.

In the present study the usefulness of a large eddy simulation for transition is examined, using the numerical code developed by Versteegh and Nieuwstadt [13]. As a continuation of previous research [2] this report describes a comparison between experiments as performed by Blom [3] and numerical simulations. The goal of the present study is to determine if a large-eddy simulation (LES) and/or a direct numerical simulation (DNS) with an equidistant grid can solve the experimentally obtained flow and to what extent a DNS can serve as a guideline to validate LES.

2 Experimental and Numerical Starting-points

2.1 The Experimental Setup

The experiments, as performed by Blom [3], were carried out with a testcell as depicted in figure 1. This testcell consists of a container with sidewalls made of

P.R. Voke et al. (eds.), Direct and Large-Eddy Simulation I, 399–410.

10 mm thick glass and top and bottom confinement designed as heat exchangers. The top heat exchanger and the aluminium elements were positioned to enclose a volume w×d×h of 150 × 90 × 100 mm. The heat exchangers were fed by water, adjusted to a prescribed temperature within ± 0.1 K in external thermostat baths. The aluminium elements were provided with threaded boreholes for the support of thermocouples.

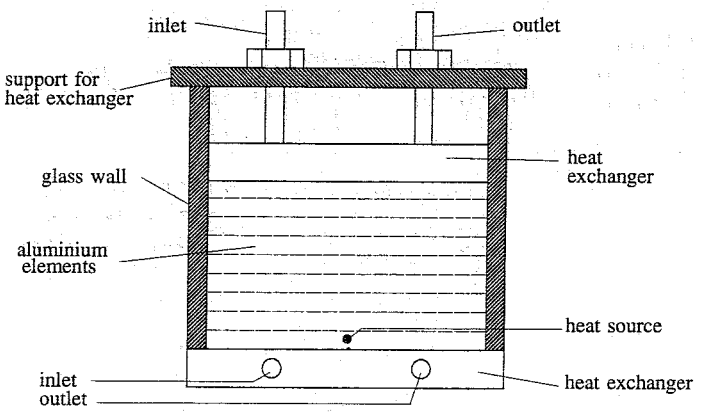

Fig. 1. The design of the testcell

In the situation considered, an electrical resistor with diameter of 5mm and length 40 mm of 22 Ω± 0.5 % was placed at the bottom of the testcell. Its length orientation was in the direction of the aluminium elements, positioned approximately at the middle of the bottom (in both directions). Insulation was placed between the resistor and the bottom. By applying a voltage of 10 V a current of 0.45 A was supplied leading to a heat flux of 4.5 W. The initial temperature of the water in the container was 301.8 K. The top and bottom heat exchangers were now connected to the same thermostat bath, adjusted to this temperature. The total flow rate through the heat exchangers was $1.33 \cdot 10^{-4} m^3/s$.

2.2 Governing Equations

The numerical code used is based on the non-dimensional Navier-Stokes equations. A characteristic velocity scale can be obtained by balancing the convective and diffusion terms of the energy equation and assuming a characteristic length scale L. In this way no assumptions have to be made about the relative importance of the mutual terms of the momentum equation, which can all be of the same order of magnitude in turbulent flows. This gives: $u_i = \frac{\kappa}{L} u_i^*$, $x_i = L x_i^*$, $t = \frac{L^2}{\kappa} t^*$, $p = \frac{\kappa^2}{L^2} p^*$ and $\theta = T / \left(\frac{q'' L}{k}\right)$ where the quantities denoted with the superscript * are non-dimensional. This superscript shall be omitted further on in this text.

The heat flux is denoted by q'' and κ and k are the thermal diffusivity coefficient and the heat conduction coefficient respectively.

By applying these relations, the non-dimensional form of the Navier-Stokes equations in Boussinesq's formulation reads:

$$\frac{\partial u_i}{\partial x_i} = 0 \tag{1}$$

$$\frac{\partial u_i}{\partial t} + \frac{\partial}{\partial x_j}(u_i u_j) = RaPr\theta\delta_{i3} - \frac{\partial p}{\partial x_i} + \frac{\partial}{\partial x_j}\left(Pr\frac{\partial u_i}{\partial x_j}\right) \tag{2}$$

$$\frac{\partial \theta}{\partial t} + \frac{\partial}{\partial x_j}(u_j\theta) = \frac{\partial^2 \theta}{\partial x_j^2} \tag{3}$$

By defining the characteristic temperature difference as: $\Delta T = q''L/k$ the Rayleigh number can be written as Ra_q (this is consistent with the non-dimensionalisation of the temperature in the energy equation (3)):

$$Ra_q = \frac{g\beta L^4 q''}{k\kappa\nu} \tag{4}$$

The Rayleigh number as defined in this way with coefficients defined at 30° C is Ra_q=$2.7 \cdot 10^{11}$, the Pr number, defined as $Pr = \nu/\kappa$ is equal to 5.82. The local Ra number in the region of the heat source, which is defined by $L = d$ had a value of Ra_q=$3 \cdot 10^5$

In direct numerical simulations these equations are solved numerically on a grid of sufficient resolution.

In the case of large-eddy simulation these equations are spatially filtered. The filtering procedure introduces an extra diffusion term, both in the momentum (2) and energy equation (3). These terms represent the influence of subgrid scale motion on the grid scale motion, and thus have to be modelled:

$$\mathcal{D}(u) = \frac{\partial \tau_{ij}}{\partial x_j} \qquad ; \qquad \mathcal{D}(T) = \frac{\partial h_j}{\partial x_j} \tag{5}$$

Now the filtered Navier-Stokes equations can be solved on a relatively coarse grid, resulting in the solution for the large scale components of the considered variables.

2.3 The Numerical Method

The numerical method consists of solving a Poisson equation for the pressure on an equidistant staggered grid at every time-step as proposed by Harlow and Welch [5]. The Poisson equation is obtained by taking the divergence of the momentum equation. The divergence of the time dependent term is discretized in time and used to force the solution to a divergence free flow field. The spatial discretization scheme is based on central differences. The time integration is carried out by a leap-frog

scheme. To avoid time splitting of the solution a weak time filter (Asselin [1]) is applied after each time step. The numerical code was developed by Versteegh and Nieuwstadt [13] and an extended description is given in Bastiaans [2]. A similar approach can be found in Schmidt and Schumann [11]. The accuracy of the numerical scheme was tested by comparison with a spectral element method as performed by Minev et al. [9]. A 2-D, unsteady, laminar plume was simulated. The difference between the midpoint vertical velocities and temperatures was within 2.5 %. More details are given in Minev et al. [9].

2.4 Boundary Conditions

On all walls of the testcell a no-slip boundary condition was applied. The 10 mm thick vertical walls of glass were assumed to be adiabatic. For the temperature at the top and bottom walls a Dirichlet condition was applied. This leads to the following set of boundary conditions: All boundaries, $u_i = 0$ and $\partial p/\partial n = 0$; Top and bottom, $\theta = 0$; Vertical walls, $\partial\theta/\partial n = 0$; Heat source, $\partial\theta/\partial n = -1$, in which n is in the direction normal to the boundary under consideration.

As mentioned before the governing equations are numerically evaluated on equidistant staggered grids. The standard grid for three dimensional calculations was of size $60 \times 40 \times 36$ of internal volumes and 60×36 for the two dimensional simulations. In the latter case grid refinement with factors 2 and 3 were applied.

Since we have an equidistant code written in Cartesian coordinates the cylindrical electric resistor could not be discretized in detail. Due to this code limitation the source was projected on the bottom of the enclosure.

2.5 Models

In turbulent flows the viscous dissipation primarily takes place at the smallest scales of motion. The effects of these scales are modeled by applying a functional relation between the subgrid scale stresses τ_{ij} or fluxes h_j and the resolved scale variables. The simplest and most commonly used models are those that are based on gradient diffusion: $\tau_{ij} = 2\nu_T S_{ij}$, and $h_j = \nu_H \partial T/\partial x_j$ in which an eddy viscosity ν_T and an eddy diffusivity ν_H are defined. The resolved scale deformation rate tensor S_{ij} is given by: $S_{ij} = \frac{1}{2}\left(\partial u_i/\partial x_j + \partial u_j/\partial x_i\right)$.

The eddy coefficients ν_H and ν_T depend on the local intensity of the turbulence. To determine the eddy viscosity a model proposed by Smagorinsky [12] in which the eddy viscosity is set proportional to the local large scale velocity gradient is widely used:

$$\nu_T = (C_s \Delta)^2 |S| \tag{6}$$

Here C_s is a constant, the filter width Δ is a characteristic length scale of the smallest resolved eddies and $|S| = \sqrt{2 S_{ij} S_{ij}}$ is the magnitude of the large scale strain rate tensor. The values of C_s that are used in large eddy simulations vary in the range $C_s = 0,07 - 0,24$, see Schmidt and Schumann [11].

A more complicated model has been used by Nieuwstadt and Moeng [10] for

natural convection flows in the planetary boundary layer. They define the turbulent viscosity in terms of the subgrid energy e:

$$\nu_T = C_\mu \Delta \sqrt{e} \tag{7}$$

for which a separate differential equation has to be solved. More details are given in Versteegh et al. [13], Schmidt et al. [11] and de Korte et al. [6].

The subgrid heat fluxes are generally modeled analogous to the subgrid stresses. Most frequently the coefficients are therefore related to each other: $\nu_H = \nu_T / Pr_T$, where Pr_T is the turbulent Prandtl number with value $Pr_T = \frac{1}{3}$.

3 The Experiment

3.1 Liquid Crystal Thermography

For the visualisation of the temperature field in the experimental situation, Blom [3] used encapsulated liquid crystals of type BM 100/R29C4W/S33, manufactured by Hallcrest Poducts Inc.. The red start of these encapsulated liquid crystals lies at 302.1 K (29° C) and they have a bandwidth of 4 K. The bandwidth is defined as the temperature difference between the blue start at cooling and the red start at heating the encapsulated liquid crystal. The average diameter was $100\mu m$ and the concentration was 0.04 % Vol. in demineralized water.

The temperature fields were visualized in a two-dimensional cross-section of the testcell. Using a 75 W Xe-arc lamp as a lightsource a parallel lightsheet was obtained with three lenses and a slit. The quality of this lightsource caused the loss due to dispersion to be minimal.

The images of the natural convective flow in the testcell were postprocessed with the software package Dig*Image*. In this way the structure of the temperature field could be determined.

In figure 2 the structure of the temperature field is presented as obtained by the liquid crystal technique. The instantaneous structure at three time levels is presented. The figures show an initial mushroom shaped structure, consisting of a dipole with a feeding boundary layer. This boundary layer could not be visualized because the temperatures in it were higher than the blue start temperature of the liquid crystals. The structure collides with the top wall and spreads out. After 60 seconds the structure didn't change much for the next 5 or 10 minutes.

3.2 Temperature Measurement

As a second feature of the flow the temperature in the middle of the cell was recorded using a thermocouple, giving additional information about the actual temperatures. Chromel-Alumel thermocouples of type K-100 with an accuracy of $\pm$ 0.1 K were used. The data was supplied to a personal computer with a sampling frequency of 5 Hz.

The result of the temperature measurement is given in figure 3. After $\pm$ 13 seconds the head of the mushroom shaped structure reached the thermocouple

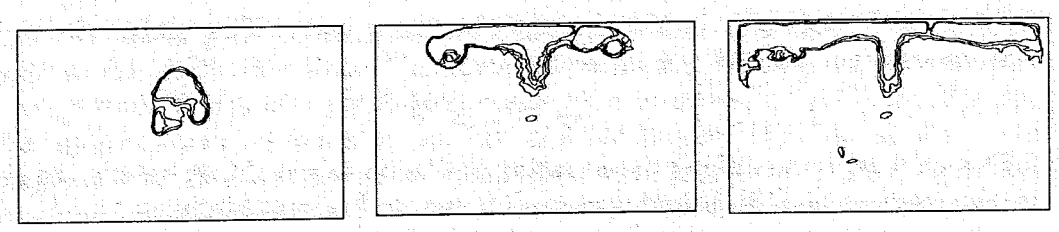

Fig. 2. Structure of temperature field at t=17, 34 and 60 sec.

and the temperature increases. In the wake of the dipole the temperature drops. The measured temperature increases again as the dipolar structure has reached the top of the testcell. Now a constant feeding boundary layer establishes and the temperature remains at a higher level of 1 - 2 K. The zero temperatures in the figures correspond with the initial temperature in the testcell, measured to be 301.8 K.

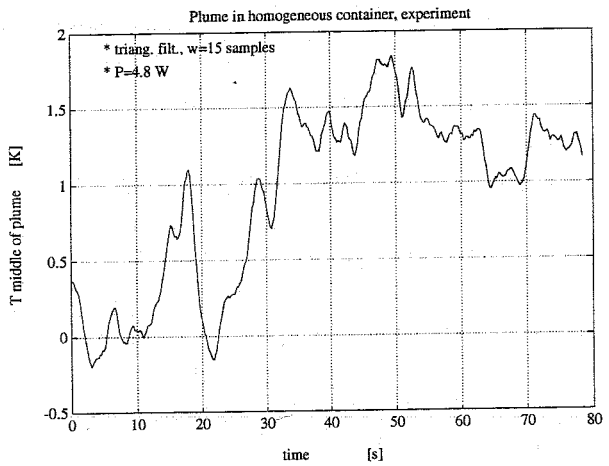

Fig. 3. Temperature in the centre of the box

4 Simulations

4.1 2-D DNS Grid Refinement Study

In order to perform a grid refinement study the problem was considered two dimensional. This was necessary in connection with the amount of computing time that would be involved. A comparison of the DNS between the three dimensional case

on the coarse grid ($60 \times 40 \times 36$) and a two dimensional slice of it (60×36) shows very little difference. The main difference is that at later times the structures in the upper left and right corners are less extended in the three dimensional case. This because of the fact that in the two dimensional situation there is no spreading out of the plume in the third dimension.

The refinement involved the basic slice (60×36) (c), two times (120×72) (m) and three times (180×108) (f) this grid size. The top picture of figure 4 is a plot of the temperature in the middle of the domain as function of time. When refinement is applied, the mushroom shaped structures arrive at later times at this location. The boundary layer breaks up in more and more concentrated blobs giving rise to high temperature and velocity peaks. The vertical velocity is displayed in the lower plot of figure 4. The delay of the temperature and velocity increase in the midpoint is caused by the fact that the initial dipole is driven apart by the boundary layer as can be observed in the first two images of figure 5. On the top of the boundary layer a new dipole is formed, which travels to the upper wall.

The differences with the experiment in the two-dimensional simulations grow with grid refinement. With the grid refinement (of three times the basic grid) the solution gets sufficiently smooth, except in the neighbourhood of the heat source. In the two dimensional (120×72) simulations the heat source was represented by 9 and 10 grid distances. The 9 panels wide source resulted in a solution dominated by spatial numerical oscillations. In the other case (a 10 panels wide source) a solution was obtained with a swaying motion of the boundary layer in the lateral direction, which is also observed in experiments.

By detailed inspection of the flow near the heat source it was found that the source and the flow in the neighbourhood of it could not be represented accurately. Numerical oscillations dominate the flow in this region, probably due to the stepwise change in boundary conditions they become more severe at smaller grids. This leads to the forming of blobs on a macroscale as can be seen in figure 5. Research is necessary to evaluate the appropriate discretization of the source.

4.2 Large-Eddy Simulations

4.2.1 Two Dimensional Calculations

In the two dimensional case large-eddy simulations were performed with the Smagorinsky model and the energy equation model with constants $C_s = 0.1$ and $C_\mu = 0.12$. The standard grid (60×36) was used.

The Smagorinsky model resulted in a solution comparable to the outcome of the 2D simulation without subgrid scale model, performed on the same grid. The topology of the temperature field and the velocities in the center of the flow domain were almost the same. The temperature, however, didn't contain peaks as large as in the no-model case, and the mean value was lower. At later times negative temperature peaks entered the negative value area frequently.

Use of the energy equation model resulted in very smooth temperatures and velocities as function of time. In the beginning the structures of the temperature

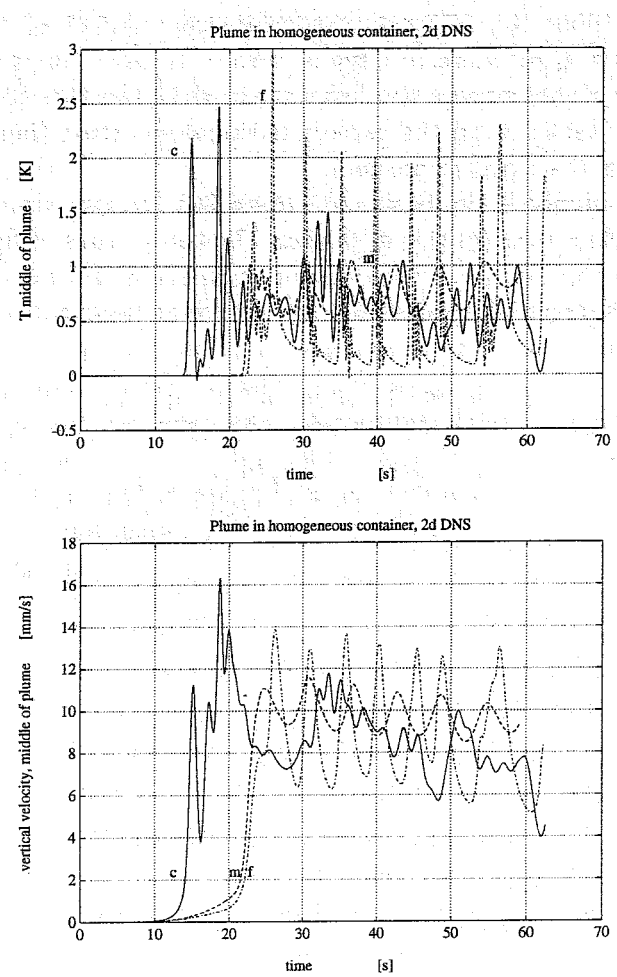

Fig. 4. Influence of grid size on local temperature and velocity, 2-D DNS

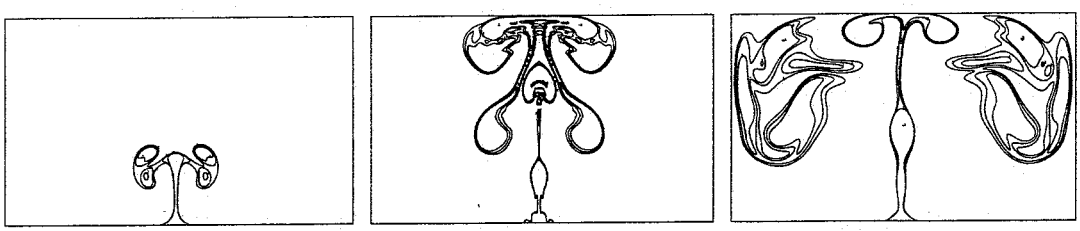

Fig. 5. Topology of the temperature field, 2-D DNS (180x108), at t=17, 34 and 60 sec.

field look very similar to those obtained by experiment, see figure 6. The diffusivity (introduced by the subgrid scale model) is higher leading to more extended structures. The differences at later times are caused by the two dimensionality. The large-eddy simulations agreed better with experiments than the DNS did, when the subgrid scale diffusivity was sufficiently large, because then numerical oscillations that disrupted the flow were not present anymore.

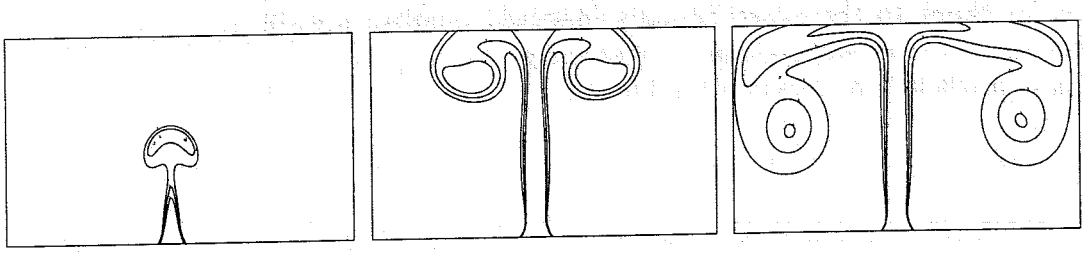

Fig. 6. Topology of the temperature field, 2-D energy equation model, at t=17, 34 and 60 sec.

4.2.2 Three Dimensional Cases

In simulating the three dimensional configuration the point of departure is again a grid containing $60 \times 40 \times 36$ volumes and a heat source discretized by 5×21 volume sides. Initially the same model constants were used as in the 2-D case. All features in the initial period of the simulation in the three dimensional case match quite well with those of the 2D configuration. The structure near the top wall is less extended due to the three dimensional spreading of the plume. Use of the standard energy equation gives a smooth solution that matches the large scale features of the experiment quite well, see figure 7. The outcome of the Smagorinsky model with coefficient $C_s = 0.1$ shows the same blobs and/or wiggles as in the no-model case.

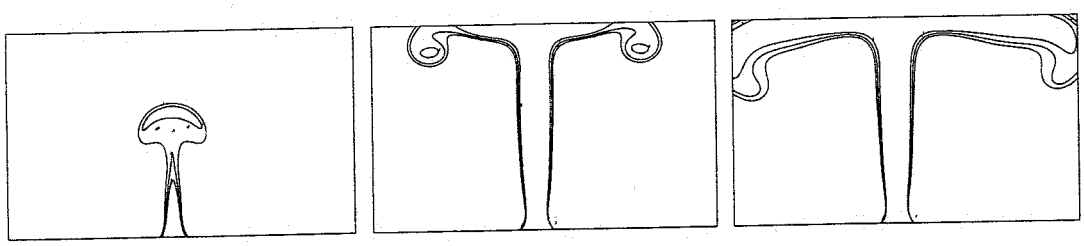

Fig. 7. Topology of the temperature field, 3-D energy equation model, at t=17, 34 and 60 sec.

By modifying the Smagorinsky constant to a value of $C_s = 0.2$ a solution was obtained matching almost exactly the solution of the standard energy equation

model. The vertical velocity in the boundary layer was slightly larger and the temperature somewhat lower.

In figures 8, 9 and 10 the differences are shown between results obtained by using the Smagorinsky model with a constant of 0.1 and 0.2 and the subgrid energy model with a constant of $C_\mu = 0.12$. Using the Smagorinsky model with a constant of 0.1 results in a very low diffusion coefficient. This is associated with numerical oscillations. However, the temperature in the midpoint after $t \approx 30$ sec. is closer to the experimentally observed temperatures of figure 3. Due to the transport and diffusion of subgrid energy the turbulent kinetic subgrid energy model predicts a more smooth solution.

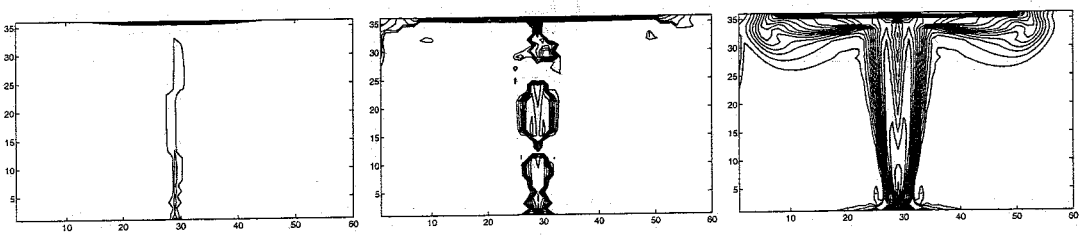

Fig. 8. Total diffusion coefficient $(\nu_T + Pr)$ (beginning at 6.5 with increments of 0.25) at t=40 sec.: from left to right: $C_s = 0.1$, $C_s = 0.2$, $C_\mu = 0.12$.

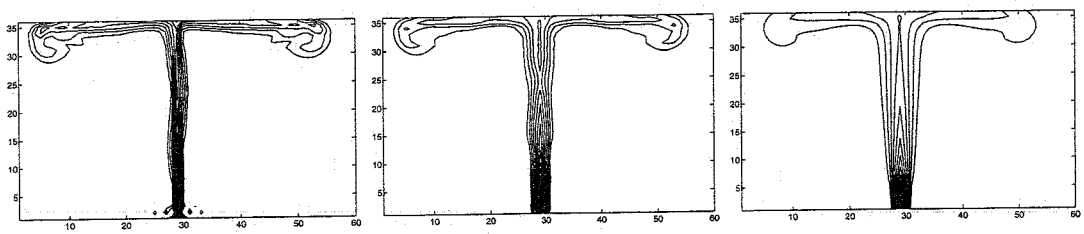

Fig. 9. Temperature (beginning at T=0.1 K with increments of 0.1 K) at t=40 sec.: from left to right: $C_s = 0.1$, $C_s = 0.2$, $C_\mu = 0.12$.

5 Conclusions and Progress

The starting behaviour of confined thermal plumes above a heat source of limited size inside a cavity with adiabatic side walls and cold top and bottom walls was investigated. Experimental results were compared to numerical solutions obtained by simulations in which different subgrid scale models and geometry configurations were used. From this study the following general features were found:

- All simulations underestimate the local temperature in the boundary layer after collision of the initial dipole with the top wall.

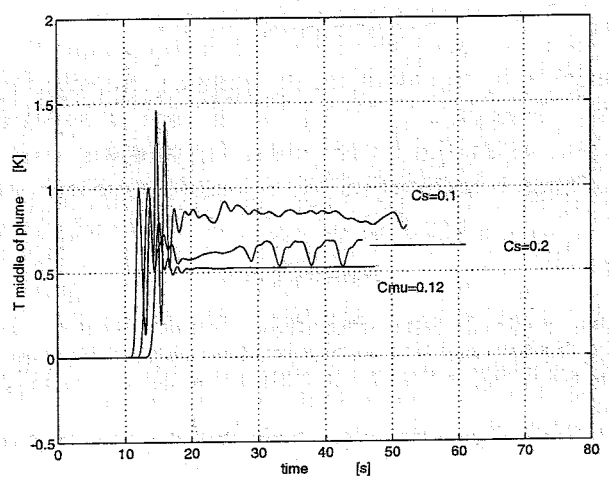

Fig. 10. Temperature in the centre of the box

- Solutions obtained by DNS show much too large temperature peaks corresponding to numerical gridsize oscillations near the source.

- Three dimensional calculations showed better results than 2D configurations, mainly due to the three dimensional spreading of the plume at the top wall.

From these points of view it can be concluded that the subgrid scale diffusivity in the large-eddy simulations was too large to predict the temperature and velocity profiles in the boundary layer. This feature is inherent to the basic idea of the subgrid scale models. The grids in the case of direct numerical simulations were too coarse. Application of a second order upwinding technique in the case of DNS would eventually prevent the mentioned numerical oscillations.

By tuning the constant in the large-eddy models the outcome of the calculations could be improved. By doing this it was found that with the energy equation model and the Smagorinsky model the same results could be obtained. Indeed, if transport of subgrid energy is of minor importance, the models are basically the same. By decreasing the constant the results were improved. It is expected that with different geometries, Rayleigh numbers and Prandtl numbers, different model constants give the best result.

The Germano model [4], a subgrid scale model in which the model coefficient is computed dynamically, will be used in a subsequent study. It is an eddy viscosity model developed to simulate intermittent and non-homogeneous flows as in the transitional case. The performance of this model in the case of transitional natural convection flows will be investigated. It will be used in the form as described by Lilly [7]. Also the performance of the structure-function model as proposed by Métais and Lesieur [8] will be examined.

Acknowledgements

This work was sponsored by the Stichting Nationale Computerfaciliteiten (National Computing Facilities Foundation, NCF) for the use of supercomputer facilities, with financial support from the Nederlandse Organisatie voor Wetenschappelijk Onderzoek (Netherlands Organization for Scientific Research, NWO).

References

1. R. Asselin. Frequency filter for time integrations. *Monthly Weather Rev.*, 100:487–490, 1972.
2. R.J.M. Bastiaans. Transitional free convection flows induced by thermal line sources. EUT Research Reports 93-W-002 ISBN 90-386-0302-9, Eindhoven University of Technology, the Netherlands, 1993.
3. G.J. Blom. Encapsulated liquid crystals as temperature indicators in thermally driven flows. Master's thesis, Eindhoven University of Technology, the Netherlands, 1993. WOC-WET 93.015.
4. M. Germano, U. Piomelli, P. Moin, and W.H. Cabot. A dynamical subgrid-scale eddy viscosity model. *Phys. Fluids A*, 3(7):1760–1765, 1991.
5. F.H. Harlow and J.E. Welch. Numerical calculation of time-dependent viscous incompressible flow of fluid with free surface. *The Physics of Fluids*, 8(12):2182–2189, 1965.
6. P. de Korte, J.G.M. Eggels, and F.T.M. Nieuwstadt. The influence of the initial conditions on freely decaying isotropic turbulence. Delft Progr. Rep. 15:103-122, Delft University of Technology, the Netherlands, 1991-1992.
7. D.K. Lilly. A proposed modification of the Germano subgrid-scale closure method. *Phys. Fluids A*, 4(3):633–635, 1992.
8. O. Métais and M. Lesieur. Spectral large-eddy simulation of isotropic and stably stratified turbulence. *J. Fluid Mech.*, 239:157–194, 1992.
9. P.D. Minev, F.N. van de Vosse, L.J.P. Timmermans, C.C.M Rindt, and A.A. van Steenhoven. 2-D DNS of unsteady plumes in a square cavity. Presented at the First ERCOFTAC Workshop on Direct and Large-Eddy Simulation, Guildford, U.K., March 1994.
10. F.T.M. Nieuwstadt. Direct and large-eddy simulation of free convection. In *Proc. 9^{th} Internat. Heat Transfer Conf., Jerusalem 19-24 August 1990*, pages 37–47. Amer. Soc. Mech. Eng., New York, 1990.
11. H. Schmidt and U. Schumann. Coherent structure of the convective boundary layer derived from large eddy simulation. *J. Fluid Mech.*, 200:511–562, 1989.
12. J. Smagorinsky. General circulation experiments with the primitive equations. *Mon. Weather Rev.*, 91(3):99–165, 1963.
13. T.A.M. Versteegh and F.T.M. Nieuwstadt. Numerical simulation of buoyancy driven flows in enclosures. Proceedings of the meeting-workshop on Mixing in Geophysical Flows, Effects of Body forces in Turbulent Flows, Barcelona, December 1992.